Chemical Engineering Journal 153 (2009) 193–198

Contents lists available at ScienceDirect

Chemical Engineering Journal

journal homepage: www.elsevier.com/locate/cej

# A macrokinetic study of the $WO_3$/Zn reaction diluted with NaCl

Hyung Il. Won, Hayk. H. Nersisyan, Chang Whan Won*

*Rapidly Solidified Materials Research Center (RASOM), Chungnam National University, Yuseong, Daejeon 305-764, South Korea*

ARTICLE INFO

*Article history:*
Received 7 January 2009
Received in revised form 26 May 2009
Accepted 28 May 2009

*Keywords:*
Combustion
Thermal profiles
Tungsten nanoparticles
Wave structure

ABSTRACT

In this work, experiments with stoichiometric $WO_3 + 3Zn$ mixture, diluted with NaCl, were conducted for nanostructured tungsten synthesis. The reaction samples, preheated until 720 K, were self-ignited and reacted in the steady combustion regime. The temperature–time profiles in the combustion wave were collected over the NaCl interval from 1 to 6 mol, and the values of the combustion parameters ($T_c$, $U_c$) were evaluated. From these profiles the spatial distributions of heat generation rate $\phi(x)$ and degree of conversion $\eta(x)$ in the combustion wave were received at different $k$ values. The calculated activation energy for the combustion process was $E = 55 \pm 2$ kJ mol$^{-1}$. After the reduction experiments, pure tungsten nanopowder with particle size from 200 to 50 nm was obtained depending on NaCl concentration.



## 1. Introduction

Investigation of the combustion mechanism of self-propagating high-temperature synthesis reactions (SHS) is of significant interest from both fundamental and practical viewpoints. The current status of computational methods and tools allows the simulation of the combustion process; however, in order to develop an adequate combustion model, it is necessary to have experimental data for each individual system, including the combustion mechanism and chemical reaction kinetics. To date, most of the knowledge on the combustion mechanism and chemical reaction kinetics occurring during the combustion of SHS systems is derived from studies of the time–temperature profiles and combustion wave structure [1–3].

Generally, the time–temperature profiles of combustion processes are measured by thermocouples, point and linear pyrometers, and 2D thermal video systems [4–6]. However, the most accurate method to obtain data on the combustion wave thermal structure is the thermocouple method. A variety of systems (borides, silicides, hydrides, etc.) were investigated by thermocouple method and the obtained results contributed to an in-depth understanding of the high-temperature kinetic and reaction mechanisms [7,8]. Two mathematical approaches have been proposed for the analysis of temperature profiles, one by Zenin [7] and the other by S.D. Dunmead et al. [9,10]. Both of them allow the extraction of the kinetic parameters of rapid combustion reactions.

Refractory oxide ($WO_3$, $Ta_2O_5$, $TiO_2$, etc.)/magnesium mixtures are of interest for the synthesis of metal nanopowders and manufacturing compact materials with dramatically improved mechanical properties for aerospace, military, chemical and metallurgy applications. Nanosized tungsten is the most promising among the refractory metals, and the commercial demand of this powder has been growing rapidly. The combustion synthesis of tungsten powder from $WO_3 + 3Zn$ system was first reported in Ref. [11]. It was shown that the reduction mechanism of $WO_3$ by Zn is multistage process including the formation of low oxides of tungsten ($WO_{2.9}$, $WO_{2.72}$ and $WO_2$) in the intermediate stages of combustion. The authors suggest that the combustion process in $WO_3 + 3Zn$ system was mainly driven by evaporation of Zn. Therefore, a decrease of combustion temperature from 1340 to 1050 K was recorded, when Zn evaporation was suppressed by an inert gas pressure. However, tungsten powder obtained under the optimized reaction conditions was mainly agglomerated and micrometer sized. We have recently reported the synthesis of nanostructured tungsten powder from $WO_3 + 3Zn$ mixture diluted with NaCl [12]. The method reported allowed to synthesize W powder with particle size less than 100 nm and an average oxygen concentration lower than 1.0 wt%.

In this article, we present an analysis of the kinetics and the combustion mechanism of $WO_3 + 3Zn + k$NaCl system as determined from temperature profiles and XRD analysis data.

## 2. Experimental

$WO_3$ powder (99.9% pure, particle size 10–50 μm; Grand Chemical and Material Co., Ltd., Korea), Zn powder (99% pure, particle size 5–10 μm; Daejung Chemicals and Metals Co., Ltd., Korea), and NaCl powder (99.5% pure, particle size <50–150 μm; Samchun Pure Chemicals Co., Ltd., Korea) were used as starting materials. $WO_3$ powder was first grinded into a fine powder (≤200 nm) and then thoroughly mixed with Zn and NaCl powders by ball-milling for at

* Corresponding author. Tel.: +82 42 821 6587; fax: +82 42 822 9401.
*E-mail address:* cwwon@cnu.ac.kr (C.W. Won).

1385-8947/$ – see front matter 
doi:10.1016/j.cej.2009.05.042

**Nomenclature**

| | |
|---|---|
| $K$ | concentration (mol) |
| $L$ | thickness (m) |
| $T_c$ | combustion temperature (K) |
| $T^*$ | maximum temperature in the reaction zone (K) |
| $U_c$ | combustion speed (cm s$^{-1}$) |
| $x$ | distance (m) |
| $Q$ | heat of reaction (J mol$^{-1}$) |
| $t$ | time (s) |
| $c$ | heat capacity (J mol$^{-1}$ K) |

**Greek symbols**

| | |
|---|---|
| $\phi(x)$ | rate of heat generation (J m$^{-3}$ s$^{-1}$) |
| $\eta(x)$ | degree of conversion |
| $\lambda$ | thermal conductivity (J mol$^{-1}$ K$^{-1}$) |
| $\rho$ | density (kg m$^{-3}$) |

*Subscripts*

| | |
|---|---|
| $c$ | combustion |
| *in.* | initial |
| *fin.* | final |

**Superscript**

| | |
|---|---|
| * | reaction zone |

least 12 h. Then, 350–400 g of the mixed powder was hand pressed into a metallic cup of 5 cm diameter and 10–15 cm length. The metallic cup with the green mixture was loaded into the box furnace and heated to 720 K (heating rate 3°/min) under a constant flow of argon gas. Self-ignition of the samples occurs near the Zn melting point (700 K). In the experiments, Λ-shaped three thermocouples consisting of Chromel–Alumel wires with 50-μm diameter were installed along with pellet to monitor temperature–time histories of burning samples. The collected temperature–time profiles and the combustion parameters ($T_c$, $U_c$) were used to deduce the steady combustion wave parameters of the reaction system.

The reaction products were treated with a dilute solution of HCl, washed with distilled water, and dried at a temperature of 320 K. Phase analysis of the reaction powders was carried out using an X-ray diffractometer (Siemens D5000) with Cu $K_\alpha$ radiation. The morphologies of the powders were analyzed using a scanning electron microscope (SEM; JEOL, Japan, JSM 5410) and field emission scanning electron microscope (FESEM; JSM 6330F).

## 3. Results and discussion

The adiabatic combustion temperature of $WO_3 + 3Zn$ mixture calculated by "THERMO" software [13] is about 1470 K. This mixture is "weakly exothermic" and dilution with NaCl renders it incombustible under ambient conditions. In order for the combustion to occur in a $WO_3 + 3Zn + k$NaCl system, it is necessary to increase the total energy content of the system. An approach to introduce an additional energy source is to preheat the reaction mixture. Therefore, basic experiments were carried out in a laboratory box furnace with a 3°/min heating rate.

### 3.1. Interaction mode

Combustion experiments performed in the $WO_3 + 3Zn + k$NaCl system (here $k$ is mole number of NaCl) revealed a strong transformation of the green mixture to the final product, when the reaction pellet was preheated to 670–720 K. It was unclear whether combustion or explosion occurred. To obtain information, three

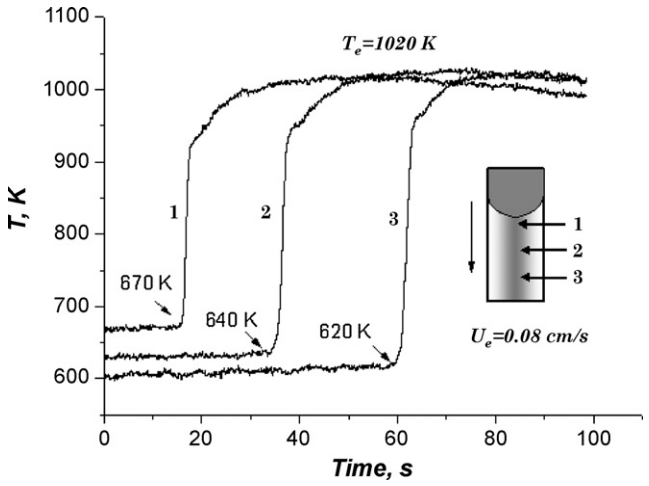


**Fig. 1.** Temperature–time profiles of $WO_3 + 3Zn + 4NaCl$ mixture.

thermocouples were installed along with the sample to collect temperature–time profiles. The typical temperature–time profiles recorded at $k = 4$ are shown in Fig. 1. These profiles are distributed in a normal range, from the top to bottom sequence, demonstrating that the interaction of the green mixture was realized in the combustion mode. It can be seen that the top surface of the specimen is heated faster due to a stream of argon blowing on the surface (convective heating). Therefore, self-ignition of the pellet occurs on the top surface at temperatures close to the Zn melting point. The combustion wave formed after the ignition propagates along with the sample, converting the green mixture into the final product. All thermocouples show a similar combustion temperature (1020 K), independent of the preheating temperature.

### 3.2. Combustion parameters

Fig. 2 shows the influence of NaCl concentration ($k$) on the combustion parameters ($T_c$, $U_c$). It can be seen that NaCl acts as a heat "sink," effectively decreasing the heat release per unit volume, maximum combustion temperature, and velocity. The lowest combustion temperature was obtained in the mixture containing 6 mol of NaCl (920 K). Note that self-sustaining regime of combustion may not be detected by thermocouples, if more than 7 mol of NaCl is applied to the starting system. Despite this fact, the sample preheated to 720–750 K shows color change from grey to bluish black indicating partial reduction of $WO_3$. The behavior of the com-

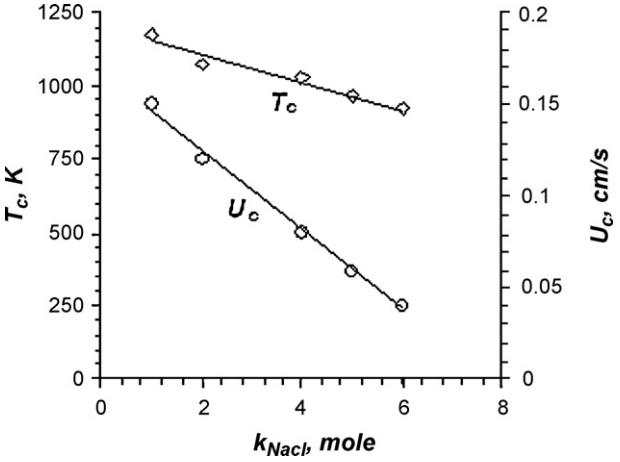


**Fig. 2.** Combustion parameters ($T_c$, $U_c$) as a function of NaCl mole concentration.

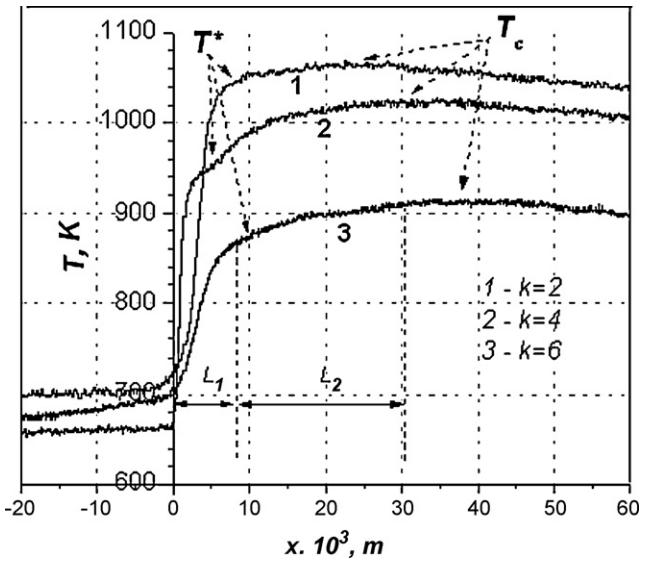


**Fig. 3.** Averaged temperature distributions in the combustion wave of $WO_3 + 3Zn + k$NaCl system.

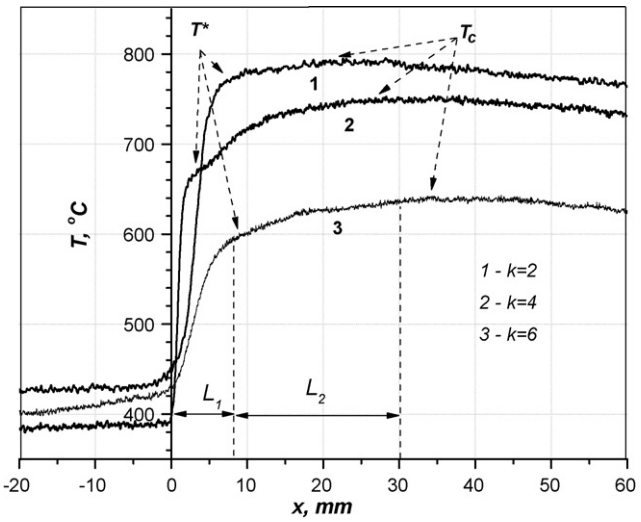


**Fig. 4.** Temperature, $T(x)$, conversion degree, $\eta(x)$, and heat generation rate, $\phi(x)$ distributions in the combustion wave of $WO_3 + 3Zn + k$NaCl system at different $k$ values.

bustion parameters of $WO_3 + 3Mg + k$NaCl system is similar to those of the diluted SHS systems [14]; however, combustion temperatures recorded in this study are low compared to those of traditional SHS redox processes. Moreover, the combustion process occurs with negligible gas release, and no sample elongation was found after the reaction. Visual observations of burned-down samples show a homogenous black-colored surface and small shrinkage in the radial direction.

### 3.3. Thermal wave structure

Averaged and smoothed temperature profiles (TPs) for $k = 2$, 4, and 6 are shown in Fig. 3. They reveal the phenomenon of a wide combustion zone composed of the reaction and afterburning subzones. There are two characteristic temperatures on these profiles: $T^*$ is the maximum temperature of the reaction zone and $T_c$ is the maximum combustion temperature. In the beginning of the reaction zone, the temperature rapidly increases to $T^*$ and then a long tail of the afterburning zone follows. According to temperature profiles data, both $T^*$ and $T_c$ decrease with NaCl concentration (Table 1). The size of the reaction zone ($L_1$) estimated from the TPs varies from $3 \times 10^{-3}$ to $7 \times 10^{-3}$ m, depending on the $k$ value. Also, the chemical processes occurring in the reaction zone are responsible for the wave propagation velocity. The afterburning zone, which is responsible for post-combustion processes, has a size $L_2$ (from $10^{-2}$ to $3 \times 10^{-2}$ m), and the wave propagation velocity cannot be affected by chemical processes occurring in this zone. The temperature–time profiles results shown in Fig. 4 indicate that the cooling process is controlled by concentration of salt. Simple calculation shows that the cooling rate of the samples has been decreasing from 3.0 to 0.5°/s, when $k$ increases from 1.0 to 6.0 mol. This may be explained by the thermal conductivity values of NaCl and W. According to the literature data, thermal conductivity of NaCl ($\lambda_{NaCl} = 4.85\ W\,m^{-1}\,K^{-1}$) is 35–40 times lower than thermal conductivity of W ($\lambda_W = 173\ W\,m^{-1}\,K^{-1}$) [15]. Therefore, the thermal conductivity with high NaCl content becomes sufficiently low, minimizing cooling rate of the sample.

### 3.4. The macrokinetic laws of the combustion process

The averaged values of the thermophysical constants of the initial mixtures and the final products are presented in Table 2. These constants were evaluated using existing data from the literature and known approximations for solid porous systems [16–18].

**Table 1**
Combustion zone parameters of $WO_3 + 3Zn + k$NaCl system.

| $k$ (mol) | $\rho$ (kg m$^{-3}$) | $U_c$ (cm/s) | $T^*$ (K) | $T_c$ (K) | $L_1$ ($\times 10^3$ m) | $L_2$ ($\times 10^3$ m) |
|---|---|---|---|---|---|---|
| 1 | 2300 | 0.15 | 1150 ± 15 | 1170 ± 15 | 3 ± 1 | 10 ± 5 |
| 2 | 2200 | 0.11 | 1040 ± 10 | 1070 ± 15 | 5 ± 2 | 15 ± 5 |
| 4 | 2200 | 0.08 | 940 ± 10 | 1020 ± 10 | 4 ± 1 | 30 ± 5 |
| 5 | 2100 | 0.06 | 890 ± 10 | 960 ± 10 | 7 ± 2 | 30 ± 5 |
| 6 | 2000 | 0.045 | 870 ± 10 | 915 ± 10 | 7 ± 2 | 30 ± 5 |

**Table 2**
Some thermophysical constants.

| $k$ (mol) | Initial mixture | | Final product | |
|---|---|---|---|---|
| | $c_{in.}\rho$ ($\times 10^{-6}$ J m$^{-3}$ K$^{-1}$) | $\lambda_{in.}$ (J m$^{-1}$ K$^{-1}$) | $\lambda_{fin.}$ ($\times 10^2$ J m$^{-1}$ K$^{-1}$) | $c_{fin.}\rho$ ($\times 10^{-6}$ J m$^{-3}$ K$^{-1}$) |
| 1 | 1.34 | 481 | 1050 | 1.55 |
| 2 | 1.3 | 481 | 1050 | 1.47 |
| 4 | 1.3 | 481 | 1050 | 1.47 |
| 5 | 1.22 | 481 | 1050 | 1.42 |
| 6 | 1.17 | 481 | 1050 | 1.34 |

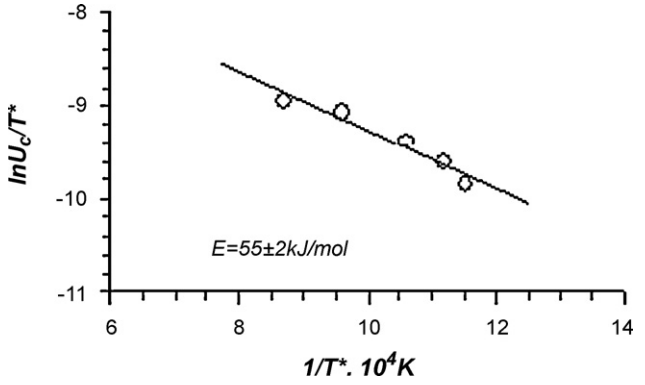


**Fig. 5.** Arrhenius plot [$\ln U_c/T^*$ vs. $1/T^*$] for the combustion process in $WO_3 + 3Zn + k$NaCl system.

The macrokinetic constants of the combustion process were calculated by the method developed in the authors' previous studies [5,19].

The equations that describe the steady combustion of SHS are as follows:

(i) equation of heat conduction:

$$\frac{\partial}{\partial x}\left(\lambda\frac{\partial T}{\partial x}\right) - mc\frac{\partial T}{\partial x} + \phi = 0 \tag{1}$$

(ii) kinetic equation:

$$-m\frac{\partial \eta}{\partial x} + \frac{\phi}{Q} = 0 \tag{2}$$

(iii) boundary conditions:

$$\begin{aligned} &x = -\infty, \quad T = T_o, \quad \eta = 0 \\ &x = +\infty, \quad T = T_c, \quad \eta = 1 \end{aligned} \tag{3}$$

The integration of Eqs. (1) and (2) result in the following expressions for $\phi$ and $\eta$:

$$\eta = \frac{mc(T - T_o) - \lambda_{in.}(dT/dx)}{(\lambda_{fin.} - \lambda_{in.})(dT/dx) + Qm} \tag{4}$$

$$\phi = mQ\frac{dT}{dx} \tag{5}$$

where $\phi$ is the rate of heat generation, $\eta$ is the degree of conversion, $Q$ is the heat of the reaction, $m = \rho U_c$ is the mass velocity of combustion, $c$ is the averaged specific heat, and $\lambda_{in.}$ and $\lambda_{fin.}$ are the thermal conductivity of the initial mixture and final product, respectively. The typical experimental curves of $\phi(x)$ and $\eta(x)$ calculated by these formulas are shown in Fig. 4. The conversion degree $\eta$ has a rapid increase in the reaction zone, conditioned by the intensive reaction of $WO_3$ with Zn. The basic part of the green mixture (from 0.6 to 0.9) transforms to the final products in this zone. The basic heat release occurs near $T^*$; the sharp peak of $\phi(x)$ corresponds to this value. This is the zone of the main heat release, which is responsible for the combustion velocity. The change of kinetic parameters in the afterburning zone is not essential.

According to the classical wide reaction zone concept, which was developed by Merzhanov [20], the combustion velocity is determined by the $T^*$, which is lower than $T_c$ (Table 1) and can be determined only from the temperature distribution. In this case, combustion velocity can be calculated from the following equation:

$$U_c^2 = AT^* \exp\left(-\frac{E}{RT^*}\right) \tag{6}$$

The activation energy of the combustion process can be derived from the experimental values $U_c$ and $T^*$ in Eq. (6); these values of

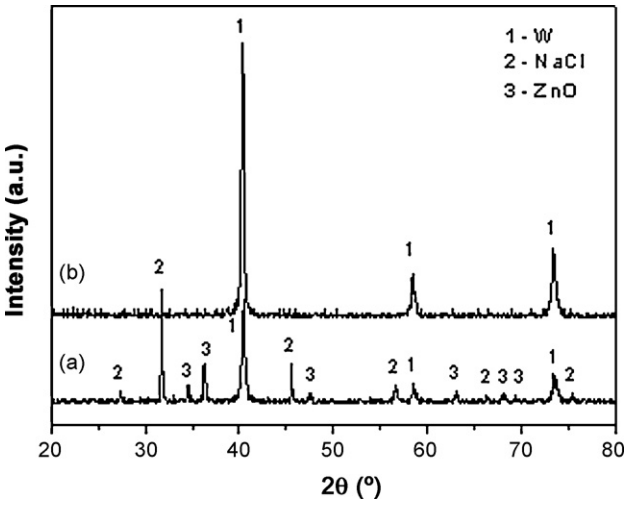


**Fig. 6.** X-ray diffraction patterns of the combustion products ($k = 4$), before (a) and after the purification (b).

$U_c$ and $T^*$ were processed in the coordinates $\ln U_c/T^* - 1/T^*$ (Fig. 5). The activation energy of $E = 55 \pm 2$ kJ mol$^{-1}$ was calculated from the slope in the plot of $\ln U_c/T^*$ vs. $1/T^*$. The low value of the activation energy seems to be attributed to $WO_3$ (solid) + Zn (liquid) mechanism of interaction because the diffusion of liquid metal into solid particles of $WO_3$ prior to the reaction has not required high activation energy.

### 3.5. Product composition and morphology

As shown in Fig. 6(a), the pattern of the final product ($k = 4$) mainly includes peaks of W, ZnO, and NaCl. After acid leaching of the final product only the peaks of W appear in Fig. 6(b). This indicates that the reduction of $WO_3$ to metallic tungsten has completed during the combustion processes. At the same time, the chemical analysis showed 1.5–4.0 wt% oxygen in the W samples, depending on the synthesis temperature. It appears that either oxygen is not chemically bonded or that the tungsten oxide phases are amorphous and cannot be detected by the X-ray technique.

Additional information about the intermediate phases of reaction, including tungsten low oxides was obtained from the samples

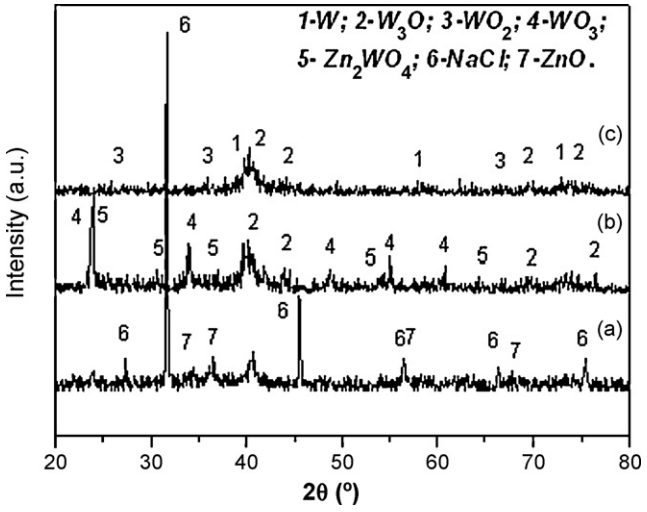


**Fig. 7.** X-ray diffraction patterns of the combustion products: (a) $k = 8$, before leaching; (b) $k = 8$, after leaching; (c) $k = 7$, after leaching.

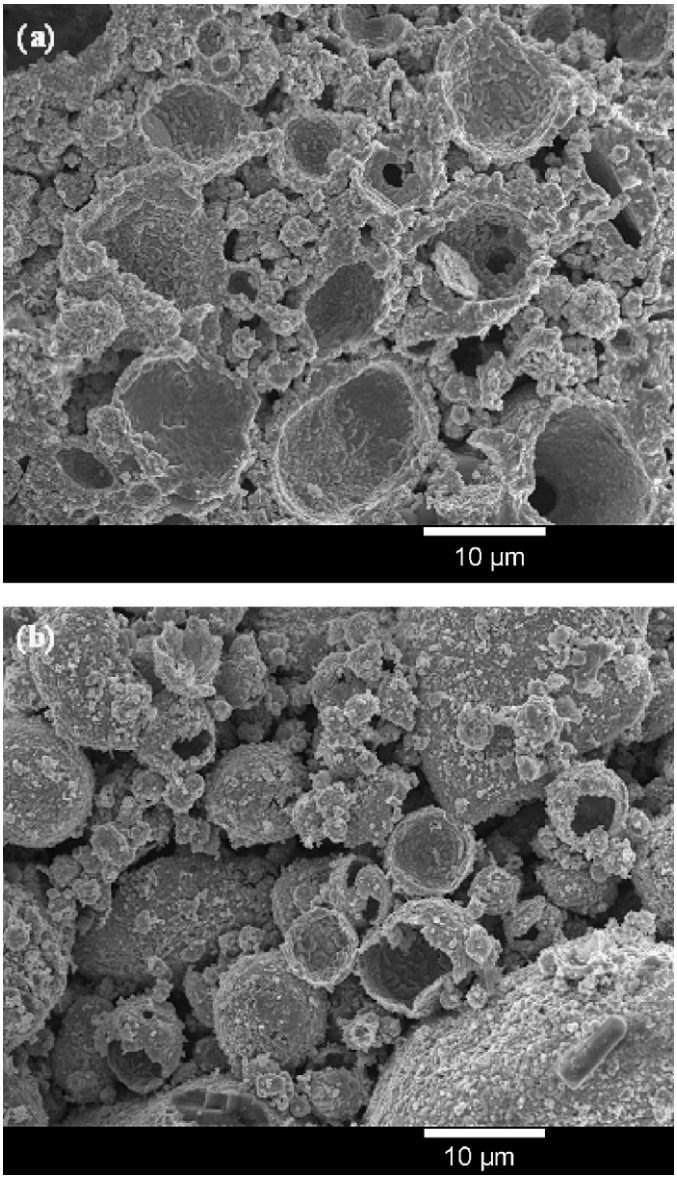


**Fig. 8.** SEM morphology of the fracture surface of the samples synthesized from $WO_3 + 3Zn + k$NaCl mixture: (a) $k = 1$ and (b) $k = 4$.

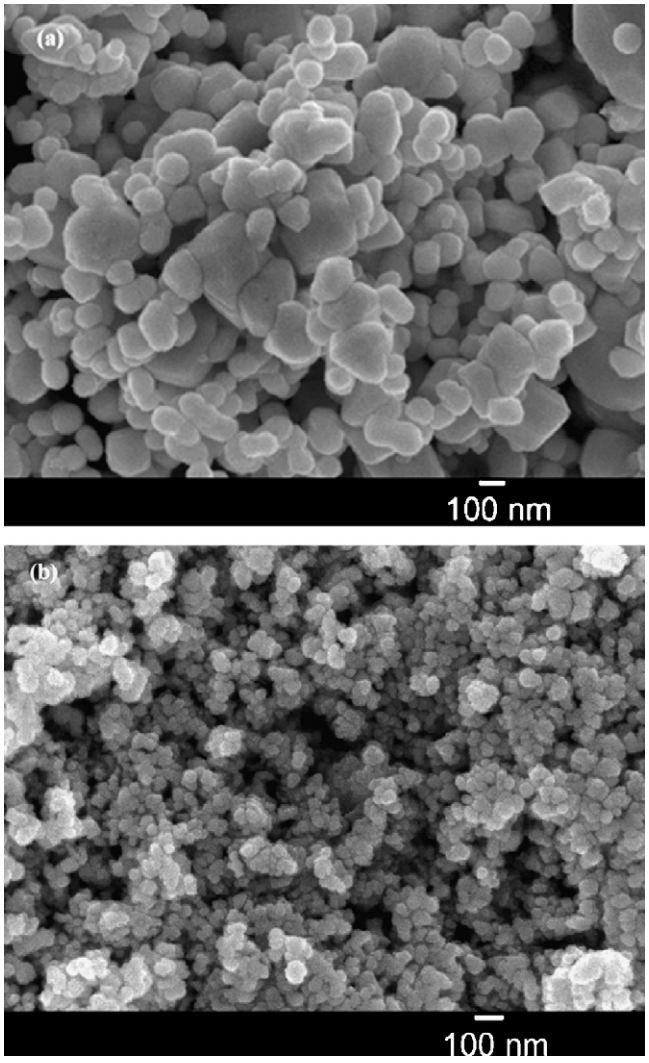


**Fig. 9.** SEM micrographs of W nanopowders synthesized at different $k$ values: (a) $k = 0$ and (b) $k = 6$.

diluted with large amount of NaCl. Fig. 7(a) demonstrates the phase composition of the final product synthesized with 8 mol of NaCl. NaCl and ZnO as major phases can be clearly seen here. However, after the dissolving of NaCl and ZnO phases, tungsten oxides ($WO_3$, $W_3O$) and zinc tungstate ($Zn_2WO_4$) have also been found in the final product (Fig. 7(b)). Diffraction peaks of $WO_3$ and $Zn_2WO_4$ were disappeared from the XRD patterns, when NaCl concentration was decreased to 7 mol (Fig. 7(c)). In this point W, $WO_2$ and $W_3O$ phases were mainly appeared after the purification.

Using these data, the reaction pathway leading to the W formation can be proposed according to following steps:

(a) 450–500 °C temperature interval:

$$WO_3 + Zn \rightarrow WO_2 + W_3O + ZnO \quad (7)$$

$$WO_3 + ZnO \rightarrow ZnWO_4 \quad (8)$$

(b) 500–600 °C temperature interval:

$$ZnWO_4 \rightarrow WO_3 + ZnO \quad (9)$$

$$WO_3 + Zn \rightarrow W + W_3O + WO_2 \quad (10)$$

(c) 600–800 °C temperature interval:

$$WO_2 + Zn \rightarrow W + ZnO \quad (11)$$

$$W_3O + Zn \rightarrow W + ZnO \quad (12)$$

The SEM morphology of the final products obtained at $k = 1$ and 4 are shown in Fig. 8(a) and (b), respectively. Hollow spherical particles can easily be seen in these micrographs. The microstructure analysis suggests that the basic reduction process of $WO_3$ occurs after the actual melting of the zinc. Consequently, this melting precedes the hollow sphere formation. The authors think that the chemical interaction between $WO_3$ and Zn first occurs on the surface of the molten zinc particles. Consequently, the shortage of zinc on the surface layer generates a concentration gradient, and the liquid zinc, under the tension forces, continuously moves from the core to the shell, resulting in hollow particle formation, as shown in Fig. 8. When the combustion temperature is higher than the NaCl melting point (Fig. 8(a)), the hollow particles of the final product become covered with molten NaCl, which is why the shell thickness of the hollow spheres is large. When the combustion temperature is lower than the NaCl melting point, the shell formation process occurs without the participation of NaCl (Fig. 8(b)). In this case, the

shell of the hollow spheres is thin and the spheres are surrounded by large solid particles of NaCl.

After acid enrichment, the hollow spherical assemblies break up, resulting in fine W powder. The micrographs of W powders prepared at $k = 1$ and 6 are shown in Fig. 9(a) and (b), respectively. As can be seen from Fig. 9(a), when 1 mol NaCl is used as diluent, it produce a higher combustion temperature (1170 K) and the particle size estimated from the micrographs is in 100–500 nm range. High concentration of NaCl produced lower combustion temperature (915 K) and approximately 50 nm sized W nanoparticles. Tungsten particles are well dispersed, because NaCl makes protective layer between W particles from the agglomeration.

## 4. Conclusions

The combustion process in a $WO_3 + 3Zn + k$NaCl system was investigated under preheating conditions using a thermocouple technique. Self-ignition of the samples close to the Zn melting point was observed. The temperature–time profiles in the combustion wave were collected over the NaCl interval from 1 to 6 mol, and the values of the combustion parameters ($T_c$, $U_c$) were evaluated. It was shown that low combustion temperatures (915–1170 K) and wave propagation velocities (0.045–0.15 cm/s) are characteristics of this system. Wide combustion zones comprised of the reaction and afterburning sub-zones were realized in the combustion wave. The distribution of the heat generation rate $\phi(x)$ and degree of conversion $\eta(x)$ in the combustion wave was received at the different $k$ values. The activation energy for the combustion process was calculated to be $E = 55 + 2\ \mathrm{kJ\,mol^{-1}}$.

The morphological study of the final products revealed the formation of micrometer-sized hollow spherical particles comprised of ZnO, W and a variable amount of NaCl. After acid enrichment, the hollow spherical assemblies broke up, resulting in fine W powder. The smallest particles about 50 nm were obtained with 6 mol of NaCl.

## References

[1] A.G. Merzhanov, Fundamentals, achievements, and perspectives for development of solid-flame combustion, Russ. Chem. Bull. 46 (1997) 1–27.
[2] A.G. Merzhanov, B.I. Khaikin, Theory of combustion waves in homogeneous media, Prog. Energy Combust. Sci. 14 (1988) 1–98.
[3] A.S. Mukasyana, A.S. Rogachev, Discrete reaction waves: gasless combustion of solid powder mixtures, Prog. Energy Combust. Sci. 34 (2008) 377–416.
[4] V.M. Maltsev, Combustion diagnostics in SHS systems, Int. J. SHS 1 (1992) 520–529.
[5] A.A. Zenin, A.G. Merzhanov, G.A. Nersisyan, Thermal wave structure in SHS processes, Combust. Explos. Shock Waves 17 (1981) 63–74.
[6] S.D. Dunmead, Z.A. Munir, J.B. Holt, Temperature profile analysis in combustion synthesis: I. Theory and background, J. Am. Ceram. Soc. 75 (1992) 175–179.
[7] A.A. Zenin, The thermal structure of solid flames, Pure Appl. Chem. 62 (1990) 889–897.
[8] A.A. Zenin, G.A. Nersisyan, Zone structure of the boride SHS wave near critical quenching conditions, Khim. Fiz. 3 (1982) 411–418.
[9] S.D. Dunmead, Z.A. Munir, J.B. Holt, Temperature profile analysis in combustion synthesis: II. Experimental observations, J. Am. Ceram. Soc. 75 (1992) 180–188.
[10] L.L. Wang, Z.A. Munir, Kinetic analysis of the combustion synthesis of molybdenum and titanium silicides, Metall. Mater. Trans. B 26 (1995) 595–601.
[11] J.H. Lee, D.H. Seo, C.W. Won, I.P. Borovinskaya, V.I. Vershinnikov, Combustion characteristics of $WO_3$/Zn reaction system in SHS process, J. Mater. Sci. 36 (2001) 5311–5314.
[12] H.H. Nersisyan, H.I. Won, C.W. Won, K.C. Cho, Combustion synthesis of nanostructured tungsten and its morphological study, Powder Technol. 189 (2009) 422–425.
[13] A.A. Shiryaev, Thermodynamic of SHS: modern approach, Int. J. SHS 4 (1995) 351–355.
[14] D.W. Lee, B.K. Kim, Synthesis of nano-structured titanium carbide by Mg-thermal reduction, Scripta Mater. 48 (2003) 1513–1518.
[15] C.W. Robert, Handbook of Chemistry and Physics, 68th ed., CRC Press, Florida, 1987.
[16] G.N. Dul'nev, L.A. Komkova, Analysis of experimental data on the heat conductivity of solid porous systems, J. Eng. Phys. 9 (1965) 517–519.
[17] E. Krumov, V. Mankov, N. Starbov, Thermal diffusivity measurements based on laser induced heat transfer in low conductive thin films, J. Opto-electron. Adv. Mater. 7 (2005) 2619–2624.
[18] M.J. Wheeler, Thermal diffusivity at incandescent temperatures by a modulated electron beam technique, Br. J. Appl. Phys. 16 (1965) 365–376.
[19] A.A. Zenin, A.G. Merzhanov, G.A. Nersisyan, The structure of the thermal wave in some SHS processes, Dokl. Phys. Chem. 250 (1980) 83–87.
[20] A.G. Merzhanov, Propagation of a solid flame in a model heterogeneous system, Dokl. Akad. Nauk. 353 (4) (1997) 504–507.